International Journal of Thermophysics, Vol. 21, No. 2, 2000

Thermophysical Properties of Molten Germanium Measured by a High-Temperature Electrostatic Levitator[1]

W.-K. Rhim[2, 4] and T. Ishikawa[3]

Thermophysical properties of molten germanium have been measured using the high-temperature electrostatic levitator at the Jet Propulsion Laboratory. Measured properties include the density, the thermal expansivity, the hemispherical total emissivity, the constant-pressure specific heat capacity, the surface tension, and the electrical resistivity. The measured density can be expressed by $\rho_{\text{liq}} = 5.67 \times 10^3 - 0.542\ (T - T_m)\ \text{kg} \cdot \text{m}^{-3}$ from 1150 to 1400 K with $T_m = 1211.3$ K, the volume expansion coefficient by $\alpha = 0.9656 \times 10^{-4}\ \text{K}^{-1}$, and the hemispherical total emissivity at the melting temperature by $\varepsilon_{\text{T, liq}}(T_m) = 0.17$. Assuming constant $\varepsilon_{\text{T, liq}}(T) = 0.17$ in the liquid range that has been investigated, the constant-pressure specific heat was evaluated as a function of temperature. The surface tension over the same temperature range can be expressed by $\sigma(T) = 583 - 0.08(T - T_m)\ \text{mN} \cdot \text{m}^{-1}$ and the temperature dependence of the electrical resistivity, when $r_{\text{liq}}(T_m) = 60\ \mu\Omega \cdot \text{cm}$ is used as a reference point, can be expressed by $r_{\text{e, liq}}(T) = 60 + 1.18 \times 10^{-2}(T - 1211.3)\ \mu\Omega \cdot \text{cm}$. The thermal conductivity, which was determined from the resistivity data using the Wiedemann–Franz–Lorenz law, is given by $\kappa_{\text{liq}}(T) = 49.43 + 2.90 \times 10^{-2}(T - T_m)\ \text{W} \cdot \text{m}^{-1} \cdot \text{K}^{-1}$.

KEY WORDS: density; electrical resistivity; electrostatic levitator; hemispherical total emissivity; molten germanium; specific heat; surface tension; thermal conductivity.

[1] Paper presented at the Fifth Asian Thermophysical Properties Conference, August 30–September 2, 1998, Seoul, South Korea.

[2] Jet Propulsion Laboratory, California Institute of Technology, Pasadena, California 91109.

[3] On leave from the National Space Development Agency of Japan; present address: Space Utilization Research Center, NASDA, 2-1-1 Sengen, Tsukuba, Ibaraki 305, Japan.

[4] To whom correspondence should be addressed.

0195-928X/00/0300-0429$18.00/0

1. INTRODUCTION

Thermophysical properties of molten semiconductors are needed for understanding liquid structures and the solidification process, and, in particular, for the numerical modeling of crystal growth processes. Although solid germanium has been rather extensively investigated, results on the properties of molten germanium are rather scarce. Even where they exist, there are substantial differences between them.

In this paper, we report measurements of thermophysical properties of molten germanium, using the high-temperature electrostatic levitator (HTESL) at the Jet Propulsion Laboratory (JPL) along with various noncontact diagnostic methods. The properties include the density, the volume expansion coefficient, the hemispherical total emissivity, the specific heat, the surface tension, and the temperature dependence of electrical resistivity. The HTESL isolates the samples from container walls through levitation in a high-vacuum condition. Under such conditions, the purity of samples can be maintained, highly undercooled liquid states are expected, and their properties can be measured using appropriate noncontact diagnostic techniques that have been developed for the HTESL.

The HTESL [1] at JPL can levitate conducting as well as semiconducting materials. Some of the characteristics of HTESL which made the present work possible are as follows. (i) It can levitate a pure germanium sample one at a time, and melt it while in levitation. (ii) The sample heating and the levitation do not interfere with each other, so that the sample can be cooled in a purely radiative manner when the heating source is either turned off or blocked. This allows a description of the whole cooling process by a well-defined heat transfer equation, making accurate measurement of c_p/ε_T possible. (iii) A levitated drop is quiescent and maintains a nearly perfect spherical shape, simplifying the processes of volume change measurement as well as the surface tension. (iv) The system is equipped with a newly developed capability of measuring electrical resistivity by applying a rotating magnetic field to a levitated sample. For some materials, this capability has an additional implication for the indirect determination of thermal conductivity through the Wiedemann–Franz–Lorenz law, which relates the electrical resistivity with the thermal conductivity.

2. EXPERIMENTAL APPARATUS AND MEASUREMENT PROCEDURES

The HTESL levitates a sample 1 to 3 mm in diameter between a pair of parallel disk electrodes spaced about 12 mm apart (Fig. 1). Four small

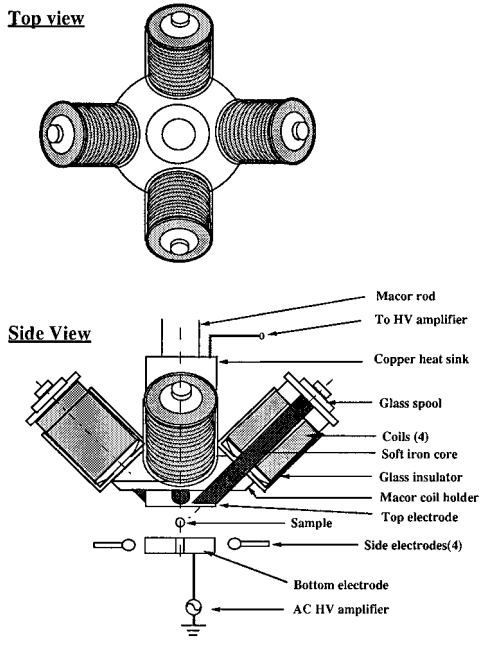

Fig. 1. Schematic diagram of the electrode assembly used in the HTESL. Four coils for sample rotation are mounted on the top electrode, and four small electrodes for lateral position control are positioned around the bottom electrode, which is electrically grounded through an ac high-voltage amplifier to induce sample oscillation.

side electrodes around the bottom electrode control the sample position along a horizontal direction, and the four coils positioned around the top electrode induce a sample rotation. The bottom electrode is connected to a high-voltage amplifier which generates an oscillating electric field to induce drop oscillation. The electrode assembly is housed by a stainless steel chamber which is typically evacuated to $\sim 10^{-8}$ torr before sample heating begins (Fig. 2). Samples are heated using a 1 kW xenon arc lamp. A detailed description of the HTESL is given in an earlier publication [1].

Once a levitated sample is molten, the melt shows a very nearly spherical shape. Germanium samples were prepared from 99.9999% pure stock from Johnson-Matthey. These were then ground roughly into spheres. They were cleaned by immersion in 5% hydrofluoric acid at room temperature for 5 min, rinsed in distilled water, and finally rinsed in anhydrous ethanol. The samples weighed approximately 20 mg.

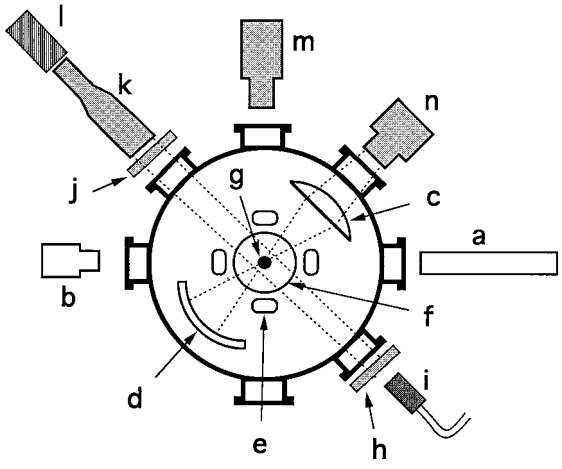

Fig. 2. Schematic diagram of the high-temperature electrostatic levitator: (a) He–Ne position-sensing laser, (b) position-sensing detector, (c) focusing lens, (d) spherical reflector, (e) side electrodes, (f) main electrodes, (g) sample, (h) light diffuser, (i) fiber optical light, (j) He–Ne blocking filter, (k) tele-microscope, (l) CCD camera, (m) pyrometer, and (n) xenon heating lamp.

Since the electrostatic levitation mechanism does not affect the sample temperature, a sample that is heated to a certain high temperature cools purely radiatively when the heating source is blocked, and the ensuing cooling process can be described by the radiative heat transfer equation

$$mc_p \frac{dT}{dt} = -\sigma_{SB}\varepsilon_T A(T^4 - T_E^4) \tag{1}$$

where m is the sample mass, c_p is the constant-pressure specific heat capacity, T is the sample temperature, T_E is the environment temperature, σ_{SB} is the Stefan–Boltzmann constant (5.6705×10^{-8} W · m^{-2} · K^{-4}), and ε_T is the hemispherical total emissivity. Since sample parameters are known and the temperature can be measured during a cooling process, one can readily obtain c_p/ε_T using Eq. (1). The fact that accurate measurement of c_p/ε_T is readily obtainable is one of the important merits of HTESL.

Measurements of the mass density and specific heat capacity of molten germanium were initiated by blocking the heating source and allowing levitated germanium melt to cool until recalescence took place. Upon beam blocking, both temperature measurement and image recording went on simultaneously throughout a cooling process. A typical temperature versus

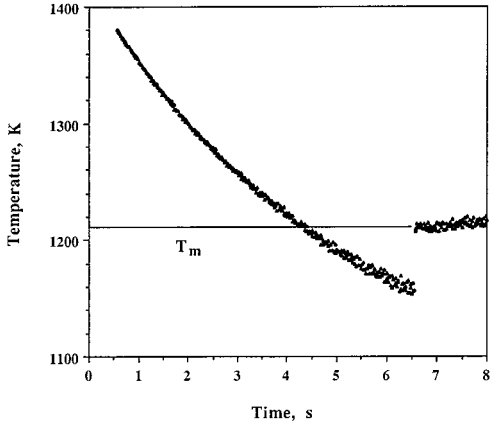

Fig. 3. A typical cooling profile of molten germanium drops during a purely radiative cooling process.

time profile for a germanium melt obtained during such a cooling process is shown in Fig. 3. The melt started to cool from about 200 K above the melting temperature and undercooled approximately 60 K before recalescence took place. Upon recalescence, the sample temperature rose sharply and reached an isothermal state. It is interesting to note that, unlike the silicon case [2], Fig. 3 shows a constant spectral emissivity over the isothermal region. The output of the single color pyrometer operating at 750 nm was calibrated by taking the temperature immediately following the recalescence as the melting temperature ($T_m = 1211$ K). The spectral emissivity of the melt at 750 nm was assumed to be constant over the liquid temperature range.

The temperature dependence of mass density was measured by analyzing the video images taken during a cooling process. The method we used in this work is basically an image analysis technique. This method consisted in (i) digitization of the recorded video image, (ii) edge detection, (iii) calculation of the area (therefore, the volume of the sample) through a linear spherical harmonic fit, and (iv) calibration of data with respect to a reference sphere for absolute values. The density was then obtained using the sample mass which was measured immediately following the experiment. A detailed description of the image analysis method used in this experiment is published elsewhere [3].

To measure the surface tension, a low-amplitude drop excitation field pulse was applied along the vertical direction, and the transient drop oscillation following the pulse was recorded in a computer for later analysis.

The drop excitation was done by applying an electric field pulse which varies sinusoidally at the drop resonance frequency. When the drop oscillation is sufficiently low in amplitude, one can utilize Rayleigh's formula to determine the surface tension from the measured resonance frequency [4]. The surface charge on a levitated drop lowers the apparent surface tension, and the drop oscillation frequency reflects this. If we know the net drop charge, we can use the Rayleigh expression for the charged drop oscillation to extract the true surface tension σ [5],

$$\omega = \left[\frac{8\sigma}{\rho r_0^3} \left(1 - \frac{Q^2}{16\pi r_0^3 \sigma} \right) \right]^{1/2} \tag{2}$$

where ω is the angular frequency of observed oscillation, ρ is the mass density of the melt, r_0 is the radius of the melt when it is in a spherical shape, and Q is the net sample charge. Effects on surface tension due to nonuniform charge distribution and deviation from a perfect spherical shape were corrected using the perturbation analysis of electrostatically levitated drops as derived by Feng and Beard [6].

3. DENSITY AND THE THERMAL EXPANSION COEFFICIENT

Accurate measurement of the density of a sample material is important since the accuracy of other thermophysical properties depends upon the accuracy of the density. Figure 4 shows the result of our density measurements

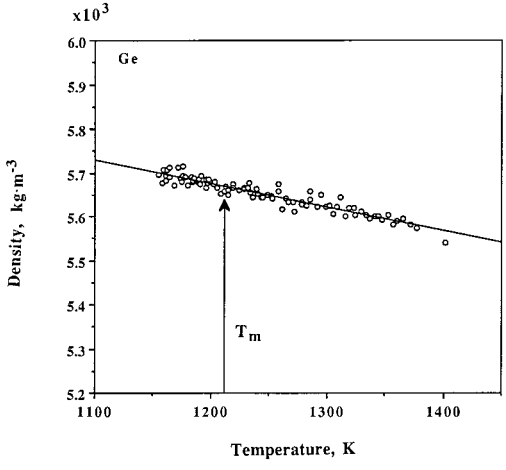

Fig. 4. Density of molten germanium as a function of temperature.

Table I. Comparison of Mass Densities of Molten Germanium

	$\rho_{\text{liq}}(T_m)$ $(10^3\ \text{kg}\cdot\text{m}^{-3})$	$d\rho_{\text{liq}}/dT$ $(10^{-1}\ \text{kg}\cdot\text{m}^{-3}\cdot\text{K}^{-1})$
Lucas [7]	5.49	−4.9
Khilya et al. [8]	5.655	−6.1
Tavadse et al. [9]	5.598	−6.25
Present work	5.67	−5.42

of molten germanium over a temperature range of 250 K. Unlike the density of molten silicon which showed pronounced quadratic behavior [2], the density of molten germanium shows a rather linear behavior which can be expressed in the following form:

$$\rho_{\text{liq}}(T) = 5.67 \times 10^3 - 0.542(T - T_m)\ \ \text{kg}\cdot\text{m}^{-3} \tag{3}$$

where the melting temperature T_m should be 1211.3 K. The estimated accuracy of this result should be better than 1%.

Table I compares the present work with three other studies which could be found in the literature. The $\rho_{\text{liq}}(T_m)$ values obtained by Lucas [7] using the bubble pressure method and by other workers using the pycnometer and volumetric measurement methods are about 2.3% smaller than our result. On the other hand, the results obtained by the sessile drop method by Khilya et al. [8] and by Tavadse et al. [9] agree with the present work within 1.25%.

However, our temperature dependence of the density gives $(\partial\rho/\partial T)_p = -5.42 \times 10^{-1}\ \text{kg}\cdot\text{K}^{-1}\cdot\text{m}^{-3}$, which is 10% larger than that of Lucas and approximately 13% smaller than those obtained by Khilya and Tavadse. For the isobaric thermal expansivity, our result is $\alpha = 0.9656 \times 10^{-4}\ \text{K}^{-1}$, which is in good agreement with $\sim 0.9 \times 10^{-4}\ \text{K}^{-1}$ given by Iida [10].

4. SPECIFIC HEAT MEASUREMENT

The constant-pressure specific heat capacity is a very important thermodynamic parameter from which other parameters, such as enthalpy, entropy, and Gibbs free energy, can be derived. In spite of their importance, the specific heat capacity and the hemispherical total emissivity are known for very few high-temperature liquids. The HTESL allows determination of $c_p/\varepsilon_{\text{T}}$ in a simple heat transfer environment while the levitated melt cools radiatively. Rearrangement of Eq. (1) gives

$$\frac{c_p}{\varepsilon_{\text{T}}} = -\frac{\sigma_{\text{SB}} A(T^4 - T_{\text{E}}^4)}{m(dT/dt)} \tag{4}$$

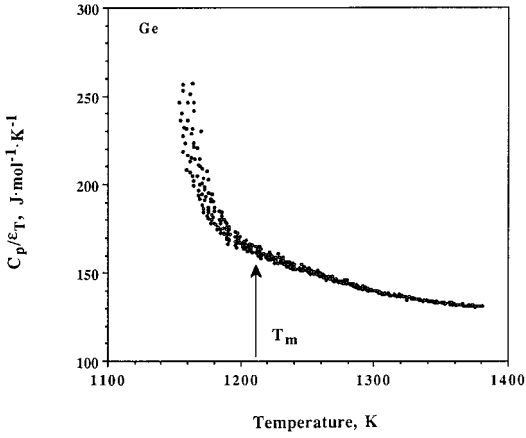

Fig. 5. c_p/ε_T vs. temperature of molten germanium as calculated from data shown in Fig. 3.

Using a temperature-time profile obtained experimentally (as shown in Fig. 3), and evaluating dT/dt from it, c_p/ε_T can be obtained as shown in Fig. 5. If all the possible experimental errors involved in obtaining these results are considered, the estimated accuracy of these data should be less than $\pm 5\%$.

From Fig. 5, $c_p(T)$ can be determined if $\varepsilon_T(T)$ is known, and, conversely, $\varepsilon_T(T)$ can be found if $c_p(T)$ is known [11]. Frequently, specific heats are known in many materials at their melting temperature, while the values for the hemispherical total emissivity are not. In such cases, $\varepsilon_T(T_m)$ at the melting temperature can be obtained. The literature value of the constant-pressure specific heat capacity of molten germanium at the melting temperature is $c_{p,\,\mathrm{liq}}(T_m) = 27.61\ \mathrm{J \cdot mol^{-1} \cdot K^{-1}}$ [12]. With this value, together with the c_p/ε_T shown in Fig. 5, the hemispherical total emissivity at the melting temperature $\varepsilon_T(T_m)$ is determined to be 0.17. This is in good agreement with Brekhovskikh's prediction that $\varepsilon_T(T)$ for the liquid will not exceed 0.18 [13, 14].

Strictly speaking, in order to evaluate $c_p(T)$, the temperature dependence of $\varepsilon_T(T)$ has to be independently measured. Since $\varepsilon_T(T)$ is not available at the present time, let us assume that it remains constant at $\varepsilon_T(T) = \varepsilon_T(T_m) = 0.17$ over the liquid region of present interest, and evaluate $c_p(T)$ from Fig. 5. Such an assumption may be a reasonable one if we consider the fact that the spectral emissivities of molten germanium at both visible and infrared wavelengths show almost no temperature dependence [15]. Figure 6 shows $c_p(T)$ as a function of temperature so obtained. Like that of molten silicon [2], $c_p(T)$ of molten germanium also shows a nonlinear behavior, decreasing with increased temperature.

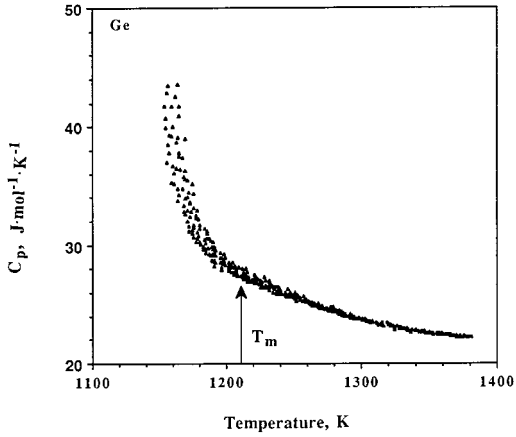

Fig. 6. $c_p(T)$ vs. temperature calculated from the result shown in Fig. 5, assuming $\varepsilon_T(T) = \varepsilon_T(T_m) = 0.17$.

5. SURFACE TENSION

The spherical shape of a molten drop levitated by the HTESL greatly simplifies the surface tension measurements. Since the surface tension is particularly sensitive to even minute surface contamination, the high-vacuum environment would be ideal for measuring surface tension, particularly of chemically reactive materials.

For surface tension experiments, we had to fix the sample temperature at a predetermined value until we obtained the surface tension data at that temperature. The pyrometer used for this experiment operated at $4\,\mu$m wavelength to avoid interference by the xenon arc-lamp radiation. As described in Section 2, a low-amplitude oscillating electric field was applied along the vertical direction, and the transient drop oscillation following the truncation of the ac field was recorded in a computer.

Figure 7 shows our surface tension results for molten germanium as a function of temperature, compared with those of Allen [16] and Takamura et al. [17]. Our surface tension data could be fit by

$$\sigma(T) = 583 - 0.08(T - T_m)\ \text{mN}\cdot\text{m}^{-1} \qquad (1160\text{–}1430\ \text{K}) \tag{5}$$

The surface tension of $583\,\text{mN}\cdot\text{m}^{-1}$ at the melting temperature is more than 6% smaller than the $621\,\text{mN}\cdot\text{m}^{-1}$ reported by Allen [16] and approximately 3% smaller than the value recently reported by Takamura et al. [17]. As for $d\sigma(T)/dT$, the present result shows $0.08\,\text{mN}\cdot\text{m}^{-1}\cdot\text{K}^{-1}$,

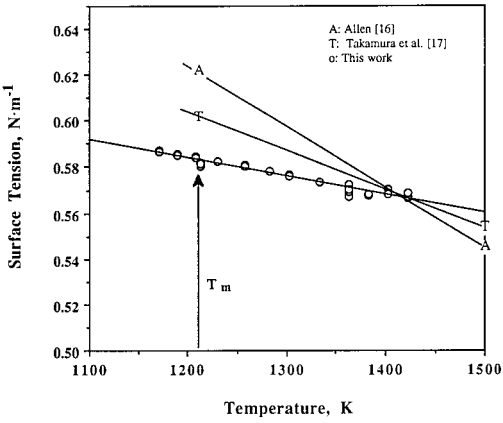

Fig. 7. Surface tension $\sigma(T)$ of molten germanium as a function of temperature.

while Allen [16] and Takamura et al. [17] found -0.26 and -0.16 $\mathrm{mN \cdot m^{-1} \cdot K^{-1}}$, respectively. The cause of such discrepancies is not known. Our levitation method in a vacuum is supposed to expose a cleaner surface, yet it is surprising that our results show smaller surface tension than the reference values. Independent control of a wider range of experimental conditions for each of the different experimental approaches should reveal the causes of such discrepancies. For a given drop surface condition, the present levitation method should be able to measure surface tension with an accuracy better than 2%.

If we measure the decay time constants of transient free oscillation signals, we should be able to relate them to the viscosity of the melt through the following relationship [18]:

$$\frac{1}{\tau_2} = \frac{5\eta}{\rho r_0^2} \tag{6}$$

In Eq. (6), τ_2 is the time constant of an exponentially decaying signal, η is the viscosity of the sample liquid, ρ is the density of the melt, and r_0 is the radius of the drop. However, we discovered that the time constant we were measuring was highly sensitive to external perturbation forces. Such susceptibility to external noise is relatively more pronounced as the viscosity of the melt decreases. In the present case, the most dominant perturbing force was coming from the levitation force correcting the sample position 480 times per second. The viscosity data we obtained scattered between 0.13 and 0.7 $\mathrm{mPa \cdot s}$ over the 1160 to 1425 K range. In contrast,

Glazov et al. [19] and Turovskii and Ivanova [20] reported 0.78 and 1.1 mPa · s at the melting point, respectively.

6. TEMPERATURE DEPENDENCE OF ELECTRICAL RESISTIVITY AND THERMAL CONDUCTIVITY

The electrical resistivity is known to be a sensitive reflection of the state of local structures in liquids. Utilizing the sample rotation capability which was newly built into the HTESL, the measurement of the temperature dependence of electrical resistivity was attempted. To exert a torque on a levitated conducting sample, a rotating magnetic field was applied to the sample with its rotation axis coinciding with the gravitational field. The basic principle is the same as the asynchronous motor in which the sample being investigated is the rotor. In fact, along with the four-probe method, the rotating magnetic field method [10] is frequently used to measure the electrical conductivity of molten material. The only difference between this method and our method is in the necessity for a container which holds the sample liquid. A sample rotation method that can measure the electrical resistivity (or conductivity) of a molten sample levitated in a high vacuum by the HTESL is truly a noncontact method.

According to the principle of the induction motor [21, 22], the torque τ is given by

$$\tau \propto \frac{s r_e}{r_e^2 + s^2 X^2} \tag{7}$$

where

$$s \equiv \frac{\omega_s - \omega}{\omega_s} \tag{8}$$

r_e is the electrical resistance of the rotor at a given temperature (the sample in the present case), X is the inductive reactance of the rotor, ω_s is the angular frequency of the applied field, and ω is the instantaneous rotation frequency of the rotor. To make Eq. (7) useful for resistivity measurements, it is important that the amplitude of the applied magnetic field experienced by the rotor remain constant for a given ω_s throughout a resistivity measurement. In the present experiment on molten germanium, the condition $r_e^2 \gg s^2 X^2$ was satisfied, so that (7) becomes even simpler, i.e.,

$$\tau \propto \frac{1}{r_e}\left(\frac{\omega_s - \omega}{\omega_s}\right) \tag{9}$$

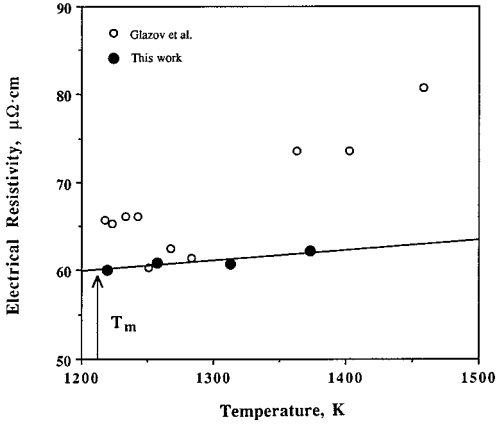

Fig. 8. Electrical resistivity of molten germanium as a function of temperature.

Once the validity of (9) was experimentally verified using a molten aluminum drop, the resistivity of molten germanium was determined by measuring the torque of a levitated sample in the neighborhood of $\omega = 0$. A detailed description of this technique will be published elsewhere [23].

Since our intent is to measure the relative electrical resistivity of molten germanium over a certain temperature range, we require a reference value at a known temperature. Keyes [24] reported $r_{\text{e, liq}}(T_m) = 0.6\,\mu\Omega \cdot \text{m}$, while $0.63\,\mu\Omega \cdot \text{m}$ was reported by Domenicali [25], and $0.6\,\mu\Omega \cdot \text{m}$ by Glazov et al. [19]. If we choose $r_{\text{e, liq}}(T_m) = 0.6\,\mu\Omega \cdot \text{m}$ to calibrate our data, our measured data can be expressed by the following equation:

$$r_{\text{e, liq}}(\text{T}) = 0.6 + 1.18 \times 10^{-4}(T - 1211.3)\ \mu\Omega \cdot \text{m} \qquad (1211.3\text{–}1380\ \text{K}) \qquad (10)$$

Figure 8 shows our results along with those of Glazov et al. While our data nicely fall onto a simple line, the data of Glazov et al. seem to show a rather complex structure. Whether such a structure has a physical meaning or is simply an expression of uncertainties involved in their experiment is not known. The accuracy of the present data should largely depend on the reference data chosen for the calibration.

Since molten germanium is a metallic liquid where free electrons are responsible for electrical and thermal conductivities, one can use the Wiedemann–Franz–Lorenz law to relate the thermal conductivity with the electrical resistivity:

$$\frac{\kappa_{\text{liq}} r_{\text{liq}}}{T} = \frac{\pi^2 k^2}{3e^2} \equiv L_0 = 2.45 \times 10^{-8}\ \text{W} \cdot \Omega \cdot \text{K}^{-2} \qquad (11)$$

where k is the Boltzmann constant and e is the electron charge. The constant $L_0 = \pi^2 k^2 / 3e^2$ is the Lorenz number, whose validity was experimentally confirmed with high accuracy by Busch et al. [26].

Using Eqs. (10) and (11), one can obtain the following expression for the thermal conductivity of molten germanium:

$$\kappa_{\text{liq}}(\text{T}) = 49.43 + 2.90 \times 10^{-2}(T - 1211.3) \ \text{W} \cdot \text{m}^{-1} \cdot \text{K}^{-1} \quad (1211.3\text{–}1380 \ \text{K}) \tag{12}$$

and Fig. 9 compares our result with two reference data available in the literature. In this figure, data from CINDAS (Center for Information Numerical Data Analysis and Synthesis) were obtained by converting Glazov's electrical resistivity data (see Fig. 8) using the Wiedemann–Franz–Lorenz law. Only Filippov's two data points were obtained through direct measurement of thermal conductivity [27]. In Fig. 8 we can observe that the choice of $r_{\text{e, liq}}(T_m) = 60 \ \mu\Omega \cdot \text{cm}$ as a reference point to calibrate our resistivity data was a reasonable one since it converts to thermal conductivity at the melting point, agreeing closely with other data. In contrast to the other two reference data, our work shows an increasing trend of thermal conductivity as the temperature increases. According to the CINDAS report, except for molten germanium, other elements in Group IVA such as tin, lead, and silicon show thermal conductivities that increase with increased temperature.

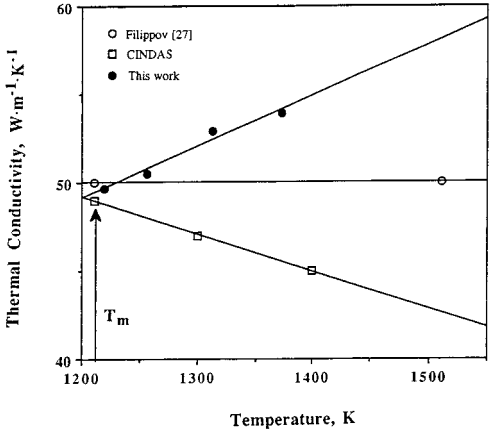

Fig. 9. Thermal conductivity of molten germanium obtained from Eq. (10) using the Wiedemann–Franz–Lorenz law. Also shown are existing reference data.

7. CONCLUDING REMARKS

In this paper, we have reported various thermophysical properties of molten germanium using different noncontact diagnostic techniques that have been developed for the high-temperature electrostatic levitator. The properties include the density, the thermal expansivity, the hemispherical total emissivity, the temperature dependence of the constant-pressure specific heat capacity, the surface tension, and the temperature dependence of electrical resistivity. The resistivity data were converted into thermal conductivity using the Wiedemann–Franz–Lorenz law.

It is noted that the present technique measures the ratio c_p/ε_T, rather than independent measurements of ε_T and c_p. Therefore, only when one of them is known can the other be determined.

We were surprised to observe that our surface tension result was smaller than the reference values by as much as 3 to 6%, although our germanium drop must have a cleaner surface. We are planning to repeat this experiment in the near future. Also, it is worth pointing out that the present approach is not an adequate means of measuring the viscosity of liquids if they have viscosities less than ~ 1 mPa · s.

The electrical resistivity measuring technique is a new addition to our HTESL. At this point, it measures only relative changes of electrical resistivity, although absolute measurement may be made possible in the future. A detailed description of this technique is beyond the scope of this paper and will be published elsewhere.

ACKNOWLEDGMENTS

The authors would like to thank Dr. Ronald H. Bogaard of CINDAS for providing several references on the thermal conductivity of molten germanium, and Daniel Barber and Dr. Paul-Francois Paradis for various assistance in this work. T.I. appreciates NASDA's generous support during his 1 year stay at JPL to conduct this research. This work was carried out at the Jet Propulsion Laboratory, California Institute of Technology, under contract with the National Aeronautical and Space Administration.

REFERENCES

1. W. K. Rhim, S. K. Chung, D. Barber, K. F. Man, G. Gutt, A. Rulison, and R. E. Spjut, *Rev. Sci. Instrum.* **64**:2961 (1993).
2. W. K. Rhim, S. K. Chung, A. J. Rulison, and R. E. Spjut, *Int. J. Thermophys.* **18**:459 (1997).
3. S. K. Chung, D. Thiessen, Y. J. Kim and W.-K. Rhim, *Rev. Sci. Instrum.* **67**:3175 (1996).
4. W. K. Rhim, K. Ohsaka, P.-F. Paradis, and R. E. Spjut, *Rev. Sci. Instrum.* **70**:2796 (1999).

5. J. W. S. Rayleigh, *Phil. Mag.* **14**:184 (1882).
6. J. Q. Feng and K. V. Beard, *Proc. R. Soc. Lond. A* **430**:133 (1990).
7. L.-D. Lucas, Liquid density measurements, in *Techniques of Metals Research IV (2)*, R. A. Rapp, ed. (Interscience, New York, 1970), p. 219.
8. Khilya, Ivashchenko, and Eremenko, *Akad. Nauk Ukr. SSR, Fis. Khim. Pov. Yavl. Raspl.* 149 (1971); cited in D. R. Lide, ed., *CRC Handbook of Chemistry and Physics*, 72nd Ed.
9. Tavadse, Khantadse, and Tsertsvadse, *Vopr. Metalloved. Korros. Met. Isdat. Metsniereba, Tiflis* (1968); cited in D. R. Lide, ed., *CRC Handbook of Chemistry and Physics*, 72nd Ed.
10. T. Iida and R. I. L. Guthrie, *The Physical Properties of Liquid Metals* (Clarendon, Oxford, 1988), p. 71.
11. A. J. Rulison and W. K. Rhim, *Metallurgical Materials Trans.* **26B**:503 (1995).
12. O. Kubaschewski and C. B. Alcock, in *Metallurgical Chemistry*, 5th Ed., revised and enlarged (Pergamon, Oxford, 1979), p. 336 (Table C1).
13. V. F. Brekhovskikh, in *Progress in Heat Transfer*, P. K. Konakov, ed. (Consultants Bureau, New York, 1966), pp. 145–150.
14. R. K. Crouch, A. L. Fripp, W. J. Debnam, R. E. Taylor, and H. Groot, in *Proc. Materials Res. Soc. Symp. on Materials Processing in the Reduced Gravity Environment of Space*, Vol. 9, G. E. Rindone, ed. (1982), pp. 657–663.
15. E. Takasuka, E. Tokizaki, K. Terashima, and S. Kimura, in *Proc. Fourth Asian Thermophysical Properties Conference*, Tokyo (1995), p. 77.
16. B. C. Allen, *Liquid Metals: Chemistry and Physics*, S. Z. Beer, ed. (Marcel Dekker, New York, 1972), p. 186 (Table 5).
17. Y. Takamura, T. Aoyama, and K. Kuribayashi, in *Proc. Spacebound 97 and 9th Int. Symp. on Exp. Methods for Micro-g Materials Science*, Montreal, Canada (1997).
18. H. Lamb, *Hydrodynamics*, 6th Ed. (Dover, New York, 1945), pp. 473–639.
19. V. M. Glazov, S. N. Chizhevskaya, and N. N. Glagoleva, *Liquid Semiconductors* (Plenum, New York, 1969), p. 61.
20. B. M. Turovskii and I. I. Ivanova, *Russ. J. Phys. Chem.* **45**:(1971).
21. S. A. Nasar and I. Boldea, *Electric Machines: Steady State Operation* (Hemisphere, New York, 1990).
22. P. L. Alger, *Nature of Induction Machine* (Gordon and Breach, New York, 1965).
23. W. K. Rhim and T. Ishikawa, *Rev. Sci. Instrum.* **69**:3628 (1998).
24. R. Keyes, *Phys. Rev.* **84**:367 (1951).
25. C. Domenicali, *J. Appl. Phys.* **28**:749 (1957).
26. G. Bush, H.-J. Guntherodt, W. Haller, and P. Wyssmann, *Phys. Lett. A* **43**:225 (1973).
27. L. P. Filippov, *Int. J. Heat Mass Transfer* **16**:865 (1973).